Electromechanical optimization of high reluctance torque variable flux machines under structural mechanical constraints

Julius Kesten [iD]
Institute of Electrical Engineering
Karlsruhe Institute of Technology
Karlsruhe, Germany
julius.kesten@kit.edu

David Armbruster [iD]
Institut für Kunststofftechnik
University of Stuttgart
Stuttgart, Germany
david.armbruster@ikt.uni-stuttgart.de

Felix Frölich [iD]
Institute of Vehicle System Technology
Karlsruhe Institute of Technology
Karlsruhe, Germany
felix.froelich@kit.edu

Luise Kärger [iD]
Institute of Vehicle System Technology
Karlsruhe Institute of Technology
Karlsruhe, Germany
luise.kaerger@kit.edu

Christian Bonten [iD]
Institut für Kunststofftechnik
University of Stuttgart
Stuttgart, Germany
christian.bonten@ikt.uni-stuttgart.de

Martin Doppelbauer
Institute of Electrical Engineering
Karlsruhe Institute of Technology
Karlsruhe, Germany
martin.doppelbauer@kit.edu

Abstract—A design approach for high speed variable flux machines with fiber reinforced polymer filled flux barriers is presented. To ensure high speed strength, the interfacial strength between the composite and electrical sheet is investigated, as it represents a strict boundary condition in the design process. A tool chain for a combination of electromagnetic and mechanical design is presented and its target values and boundary conditions are discussed. Measurements of the interfacial shear strength between electrical sheet and the composite are carried out and the results are investigated with respect to the design process. An optimization based on the measurement data is carried out and the results of machines with and without composite reinforcement are compared.

Index Terms—multi material design, optimization, high speed, rotor design, insert

I. Introduction

Modern traction machines need to be both efficient during operation as well as efficient with respect to material consumption. A machine's electric power P_{el} can be elevated by increasing either the rotating speed n, the air gap flux density $\hat{B}$ or the current loading A. While the latter of the goals above are achieved by using additional magnets or advanced cooling for larger currents, higher rotating speeds can only be reached by increasing the rotor's mechanical strength, while not decreasing electromagnetic performance. Different approaches to reinforce a machine's rotor have been presented. In [1] the authors propose a synchronous reluctance machine (SynRM) with fluid shaped barriers that are filled with an epoxy resin to improve the machine's speed strength. An extensive review of the epoxy resin's mechanical properties

is given and the selection process is described. The adhesion between resin and electrical sheet is then tested using a simplified geometry. The contact area can withstand contact pressures of $10\,\mathrm{MPa}$.

In [2], a ribless SynRM rotor is proposed and an epoxy resin is used as filler. In addition to the filled flux barriers, there are also end caps made from the resin to give additional support. Also, there are no outer webs in the rotor's flux barriers. Through the avoidance of the webs in the center and on the outer edges of the flux barriers, the machine's peak current with regard to maximum torque was reduced compared to the same geometry with these webs.

The authors of [3] chose an approach employing additional inserts in the rotor structure to improve speed strength. These inserts are made from unidirectional glass fiber composite which fulfils the function of the webs while being non-magnetic. This reduces stray flux in the d-axis while allowing for an improved maximum speed. Also, the authors provide an extensive review of further techniques to reinforce a SynRM's rotor, which is recommended for further reading.

While the concepts for increased rotor speeds and improved saliency in SynRM show conclusive results, they focus on pure SynRM only and do not take permanent magnet assisted SynRM (PMaSynRM) into account. Also, they employ either epoxy resin or inserts for which the rotor needs to be specifically designed to reach these goals.

This work therefore focuses on a PMaSynRM with AlNiCo magnets, allowing it to be used as a variable flux machine (VFM), the principle of which as well as the design process are presented in [4]–[7]. To increase speed strength, the machine's flux barriers are filled using glass fiber reinforced polyphenylene sulfide (PPS) with $40\,\%$ fiber content. It is applied into the barriers using injection molding, thus enabling

manufacturing in large quantities and better recyclability comapred to epoxy based approaches, as presented by the authors in [8]. Further, investigations into the mechanical modeling of variable flux machines were presented in [9], with the focus imposed on the quick prediction of the magnetic forces acting on the machine's airgap.

In this work, the design process with the constraints imposed by the filling of the flux barriers is presented. Section II focuses on the general design process and presents a toolchain developed for the design of VFM. The experimental data necessary to define the mechanical constraints is presented and analyzed in Section III, the rotor geometries resulting from the design process are presented in Section IV. A brief summary and an outlook on the project are given in Section V.

The focus of the work lies on the mechanical design. Electromagnetic parameters are considered and presented in part, but not as extensive as the mechanical parameters.

II. MULTI DOMAIN MACHINE DESIGN

A. Design toolchain

The design principles for the type of machine taken as a basis in this paper were presented in [8] with the concept of composite-filled flux barriers to increase speed stability. In Fig. 2, a workflow is presented to automatically determine an optimal rotor geometry for a machine design for known interfacial strengths $\tau_{\mathrm{y,I}}$.

Using latin hypercube sampling (LHS), a number k of rotor geometries is automatically created within given limits for pre-defined parameters, such as the magnets' thickness, the magnets' width, the thickness of the rotor yoke or the angle of the flux barriers. In total, 13 variable parameters are implemented in the rotor design, which is displayed in Fig. 1. Note, that for the sake of readability, parameters describing
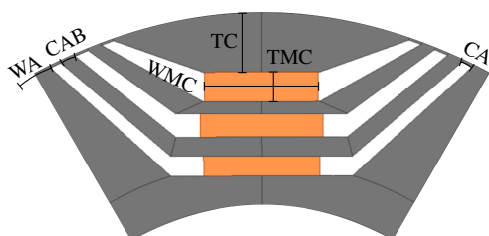

Fig. 1: Rotor base geometry.

the same geometric feature for different parts of the machine were omitted in Fig. 1. The full set of parameters as well as their respective units and the limits in which they can vary are given in Table I. Using the definition of the rotor geometry, these k designs are then evaluated both in the electromagnetic and the mechanical domain using FEA solvers. To solve the mechanical problems, Dassault Abaqus is used, while Ansys Electronics is employed for the electromagnetic calculations. The electromagnetic FEA generates information regarding the performance data of the resulting machines, the mechanical FEA delivers information regarding the speed related boundary conditions for machine operation. To improve the reliabilty

TABLE I: Parameters in the rotor design

Parameter	Description	Limits	Unit
TMA	Thickness magnet A	$[3, 4.5]$	mm
WMA	Width magnet A	$[17, 21]$	mm
TMB	Thickness magnet B	$[3, 4.5]$	mm
WMB	Width magnet B	$[17, 21]$	mm
TMC	Thickness magnet C	$[3, 4.5]$	mm
WMC	Width magnet C	$[3, 4.5]$	mm
TC	Pole cap at magnet C	$[8, 11]$	mm
WA	Pole arc between poles C	$[5, 15]$	mm
CA	Opening angle of flux barrier A	$[1, 3]$	°
CB	Opening angle of flux barrier B	$[1, 3]$	°
CC	Opening angle of flux barrier C	$[1, 3]$	°
CAB	Angle between A and B	$[1, 3]$	°
CBC	Angle between B and C	$[1, 3]$	°

of the mechanical results, the magnets' sharp corners as depicted in Fig. 1 are automatically chamfered. This avoids failures in solving the numerical problem, since the chance for singularities is reduced.

The results of both the electromagnetic and the mechanical FEA are then post-processed using MATLAB and the input parameters are set in relation to the respective output parameters using Gaussian Process Regression. Depending on the design goals selected, either a genetic or a multi objective genetic optimization algorithm from MATBLAB's global optimization toolbox is employed. The machine designs output by the optimizer are then again analyzed in FEA and the most suitable one is selected.
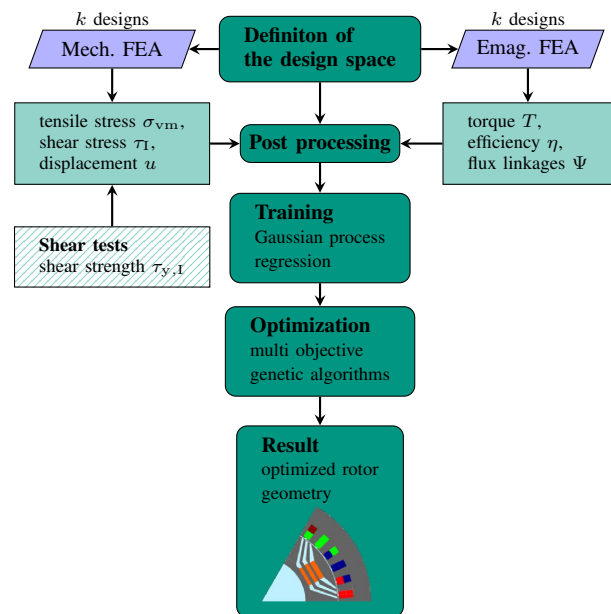

Fig. 2: Design toolchain flow chart.

B. Design restrictions

The underlying dataset for the examinations undertaken in this work consists of $k = 1000$ rotor geometries generated using LHS with a fix stator and winding design, the data of which are presented in Table II. The electromagnetic design

goals consist of the machine's output power at the corner point P_{nbase}, the output torque at the corner point T_{max} and the external fields acting on the magnets H_{err}. While the first two of these goals are maximized, the number of points beyond the magnets' BH-curve's knee point H_{err} are to be minimized, as described in [8]. The mechanical boundary conditions imposed on the system are the sheet's yield strength $\sigma_{y,S}$ and the maximum interface stress permitted $\tau_{y,I}$. The correlation

TABLE II: Characteristics of the machine under investigation

Characteristic	Value
No. of phases m	3
No. of pole pairs p	3
No. of slots N_s	36
No. of conductors per coil Z_c	4
Stator bore diameter D_b (mm)	140
Electric sheet material	NO-30
Maximum current (A)	100
DC link Voltage (V)	400

between the rotor design parameters varied in the DOE and the mechanical properties of the machine is presented in the form of a correlation matrix in Fig. 3. Here, the interaction between mechanical and electromagnetic design parameters and restrictions becomes visible. As can be seen for the middle magnet's thickness TMB, the increase of its size will likely decrease the mechanical stress in the sheet σ_{vm}, as well as the interfacial shear stress τ_I. However, it also has a negative correlation to the corner speed torque, meaning an increase of TMB will likely decrease the maximum torque as well. Another example can be made for the width of the innermost magnet WMA. Increasing the value of this parameter appears to decrease the mechanical stress overall, while increasing the number of working points with too large external fields H_{err}. The correlation between the outer magnet's thickness TMC and H_{err} shows the plausibilty of the figure. If the parameter is increased, i.e. if the outermost magnet gets thicker, the number of erroneous fields becomes smaller. Since magnet C is subjected to the largest magnitudes of external fields, the negative correlation between its thickness and H_{err} appears conclusive.

As becomes clear from the flow chart presented in Fig. 2 the load on the interface between PPS and electrical sheet in the form of shear stress τ_I is the critical mechanical design restriction. The effect of the PPS in the machine's flux barriers on the stress in the sheet can be seen in Fig. 4a and 4b, respectively, where the maximum stress on the electric sheet is presented for both the machines with reinforced flux barriers and those without for speeds of $n = 15\,000\,1/\mathrm{min}$, $n = 17\,500\,1/\mathrm{min}$ and $n = 20\,000\,1/\mathrm{min}$.

The mechanical parameters of both the electrical sheet and the PPS are listed in Table III; it shows the yield strength σ_y, the Young's modulus E and the thermal expansion coefficient α for both materials. As can be seen from the table, the thermal expansion coefficient α is similar for electrical sheet and PPS. This is important for the long term stability of the injected rotor because there is significant heat development to be
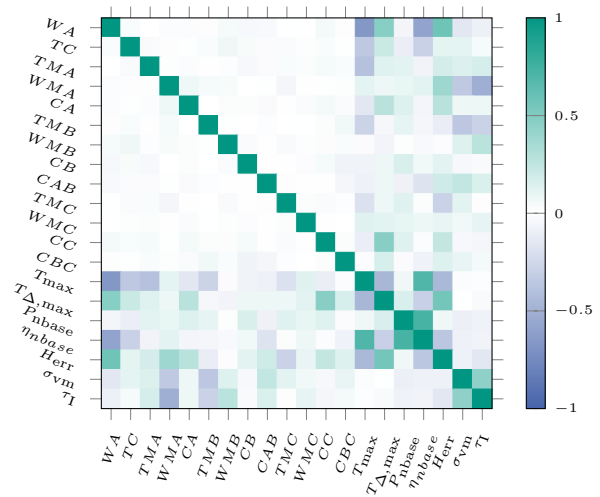

Fig. 3: Correlation matrix of mechanical and electromagnetic parameters for $n_{max} = 17\,500\,1/\mathrm{min}$.

TABLE III: Mechanical properties of rotor materials

Material	σ_y (MPa)	E (GPa)	α ($10^{-6}\mathrm{K}^{-1}$)
NO-30	420	210	13.2
PPS (GF 40 %)	180	32	14.5

expected as a result of the rotor's iron and the magnet losses. If materials with too large a difference between their expansion coefficients were used, the differences in thermal expansion might lead to a destruction of the interface. To ensure no damage is inflicted on the rotor sheet stacks during the mold injection process, simulations were carried out to optimize flow paths of the mold and to ensure an even distribution of pressure during the filling process.

Considering a typical safety factor of 1.4 the machines without the composite reinforcement would be safe to run at a maximum speed of $15\,000\,1/\mathrm{min}$ only. Through the application of the PPS the maximum stress is reduced below the sheets' yield strength for all maximum speeds considered. While $\sigma_{y,s}$ is a known parameter that can be taken from

(a) without composite   (b) with composite
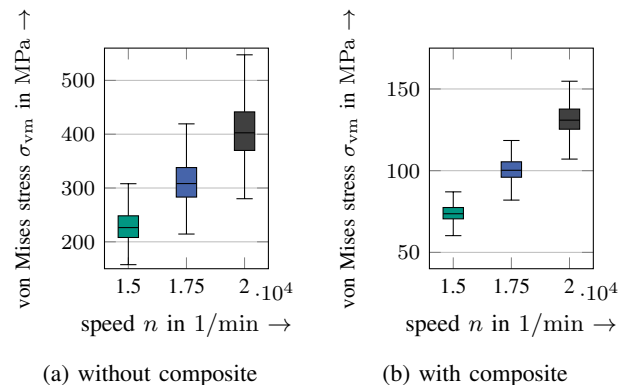
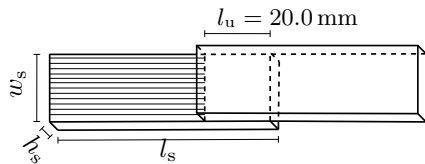Fig. 4: Simulated von Mises stress in the sheet for the $k = 1000$ rotor geometries.

Fig. 5: Schematic representation of the shear test specimen.

the material's datasheet, the maximum shear strength of the interface $\tau_{\mathrm{y,I}}$ is unknown due to the material combination.

III. Experimental Investigation of Interfacial Strength

For this reason, shear test specimens were manufactured in different configurations to determine $\tau_{\mathrm{y,I}}$. The interfaces between sheet and composite in the electric machine are approximated using rectangular stacks of electric sheets made from NO-30 with a width of $h_{\mathrm{s}} = 5\,\mathrm{mm}$, a length of $l_{\mathrm{s}} = 80\,\mathrm{mm}$ and a heigth of $w_{\mathrm{s}} = 20.1\,\mathrm{mm}$ where the height describes the direction of stacking. The resulting contact area has a size of $20.1\,\mathrm{mm} \times 20.0\,\mathrm{mm}$. A schematic of the samples is presented in Fig. 5. To ensure the highest possible joint strength, the metal specimens were pre-treated in different ways.

Firstly, the electric sheet specimens were pre-treated using plasma. Plasma coating is a chemical-physical process in which a plasma composite layer is produced on the metal body under atmospheric pressure. The coating consists of an organosilicon compound, which is added to the plasma as a precursor and is deposited on the metal. The silicon bonds with the metal or metal oxide at the molecular level. The deposited layer fills even small cavities and thus creates a high impermeability of the bond. At the same time, it serves as an anticorrosive barrier against the penetration and infiltration of water, salt solutions and gases. The organic components contained in the layer ensure the adhesion of the plastic [10].
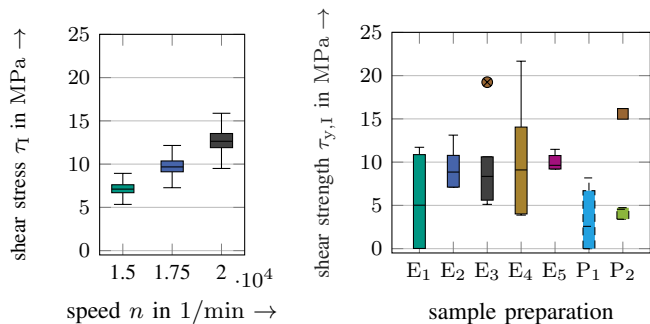
In addition, the surfaces of further electrical sheet samples were etched using nanoscale sculpturing. In this electrochemical process, whole or large parts of unstable grains are selectively removed from the surface. This produces a three-dimensional surface structure characteristic of this process. Since no grain boundaries are dissolved in the process, the advantageous mechanical properties are fully retained [11].

Preliminary tests with adhesion promoters based on aminopropytriethoxysilane showed only low interfacial strengths between metal and plastic and were therefore not pursued in further investigations.

The specimen and tool preparation is presented in Table IV, where E_i denote the etched specimen and P_i denote the specimen pre treated using plasma. The fabricated shear test specimens were tested on a ZwickRoell universal testing machine. Using the forces at break determined in this way,

TABLE IV: Tool and specimen preparation for the different shear tests

	T_{spec} (°C)	T_{tool} (°C)
E_1	260	160
E_2	280	160
E_3	300	160
E_4	280	140
E_5	280	120
P_1	280	160
P_2	300	140

(a) Calculated shear stress   (b) Measured shear strengths

Fig. 6: Interface stress and shear strengths.

the shear strength τ_{I} can be calculated according to [12]:

$$\tau_{\mathrm{I}} = F \cdot \sqrt{\frac{9 \cdot (\frac{h_{\mathrm{s}}}{2} + \frac{h_{\mathrm{s}}}{2})^2}{w_{\mathrm{s}}^2 \cdot l_{\mathrm{u}}^4} + \frac{4}{w_{\mathrm{s}}^2 \cdot l_{\mathrm{u}}^2}} \tag{1}$$

with the loading force F, the thickness of the first and second bonded material, both h_{s}, the lapping width w_{s} and the lapping length l_{u}. The calculated tensile strengths in the interface are shown in Fig. 6b while the shear stress according to the simulations is presented in Fig. 6a. The maximum simulated shear stress is $\tau_{\mathrm{I}} \approx 16\,\mathrm{MPa}$ at $n = 20\,000\,1/\mathrm{min}$, while the minimum occurs at $n = 15\,000\,1/\mathrm{min}$ with $\tau_{\mathrm{I}} \approx 5\,\mathrm{MPa}$. The results of the shear tests extend from samples which were destroyed upon insertion into the testing machine, such as the test series E_1 and P_1, to a maximum shear strength of $\tau_{\mathrm{y,I}} \approx 21\,\mathrm{MPa}$ in series E_4, which allows rotor speeds of more than $20\,000\,1/\mathrm{min}$. While the median value of the shear strength is similar with $\tau_{\mathrm{y,I}} \approx 10\,\mathrm{MPa}$ for the test series E_2 - E_4, series E_1 and both of the series of plasma treated specimen have lower median values.

The results obtained so far show etching of the electrical sheet as the most promising pre-treatment to obtain high strengths. Further improvements in interfacial strength are expected through optimization of the injection molding process. As presented in Table IV the samples need be pre-heated to bond the sheet to the PPS. Since both preheating and the etching could result in damage to the sheets' baking varnish, the electrical resistance was measured before and after the pre-treatment and preheating. No damage to the coating was detected.

IV. RESULTS

In this section the rotor geometries achieved through application of the design process described in Section II with the boundary condition defined through the experiments presented in Section III are presented and compared to a rotor geometry without composite injection optimized with the same toolchain. The maximum speed targeted is $n_\mathrm{max} = 17\,500\,1/\mathrm{min}$. The maximum value for the boundary condition of the interface stress is selected according to the upper quartile of E_4 to $\tau_\mathrm{I,max} = 15\,\mathrm{MPa}$, the maximum value for the von Mises stress in the sheet is set to $\sigma_\mathrm{vm,max} = 400\,\mathrm{MPa}$. Using these nonlinear boundary conditions, the optimization is carried out for both the data with and without composite and 77 data sets, i.e. 77 rotor geometries with values for each of the 13 rotor parameters, result from each process. Out of these 77 data sets each, the resulting machines with and without composite reinforcement are selected according to the lowest number H_err, which might not yield the highest torque T_max or the highest base speed power P_nbase, but assures operation without accidental demagnetization. The machine without composite injection is denoted as M1, while the one with composite injection is denoted as M2.

Fig. 8 presents the resulting sheet stress in both the data sets with and without the composite in the flux barriers. The stress σ_vm has similar median values compared to the data presented in Fig. 4. For the machines without composite however, there is a tendency towards higher values, while the stress σ_vm of M2 is distributed evenly. This shows the positive effect of the composite on the conflict of goals discussed in Section II-B: without composite injection, the maximization of torque and power can only be achieved with comparably high stress σ_vm in the electrical sheet, while the reinforced rotors can better withstand the mechanical load. The shear stress in M2 has a tendency towards lower values.

(a) σ_vm without FRP (b) σ_vm with FRP (c) τ_I with FRP

Fig. 8: von Mises stress of the 77 optimized machines with and without composite reinforcement (FRP) and the shear stress of those with reinforcement.

machines, the load on the electrical sheet differs by a factor of more than 3.6. The security factor for the sheet is 1.1 in the case of the machine without composite injection. The shear stress acting on the interface in the machine M1 with composite injection lies within the upper and lower quartile (see Fig. 8c), so does the stress acting on the sheet (Fig. 8b). The comparison between the geometries of M1 and M2 shows similar geometric features. However, the effect of the composite injection into the flux barriers provides a considerable amount of additional sturdiness. Further, the underlying assumption for the boundary condition of the interfacial shear stress is an instantaneous failure of the rotor, should the interface fail. This assumption might prove to be incorrect, since the composite inside of the barriers has a stabilizing effect on the electrical sheet even in the case of interface failure.

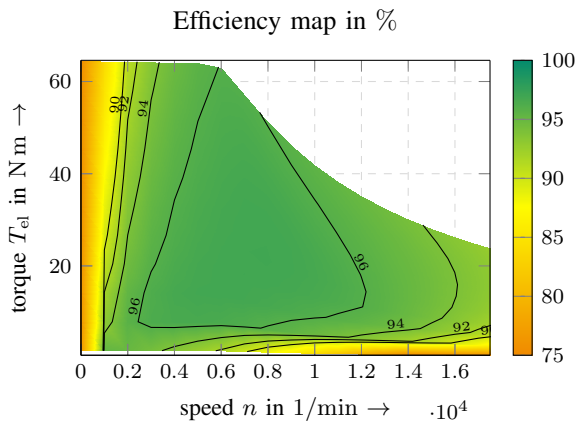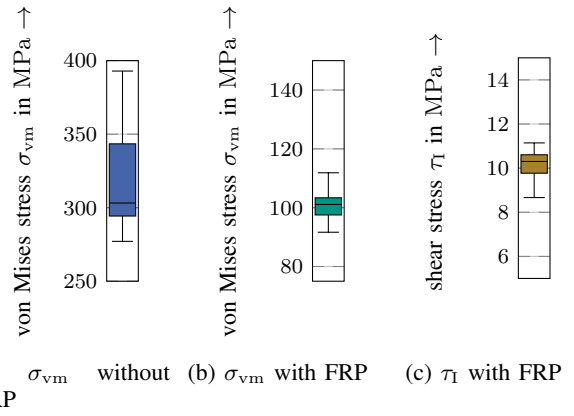The efficiency map of M2 is presented in Fig. 7.

Fig. 7: Efficiency map of the machine with composite injection.

The performance values for both selected machines M1 and M2 as well as the mechanical stress are presented in Table V. While the electromagnetic parameters are similar for both

TABLE V: Parameter data for optimized machines

Parameter (unit)	M1	M2
T_max (N m)	63.76	63.68
P_nbase (kW)	40.061	40.011
η_max (%)	96.98	96.98
H_err (–)	3	4
σ_vm (MPa)	381.2	105.57
τ_I (MPa)	–	10.46

V. CONCLUSION AND OUTLOOK

A design process for high speed variable flux machines is presented and the necessary boundary conditions for the composite filling of the flux barriers are investigated. Using the presented optimization workflow, a rotor geometry can be determined based on the preliminary results, which allow rotor speeds of up to $v_\mathrm{rot} = 127\,\mathrm{m/s}$, corresponding to $n = 17\,500\,1/\mathrm{min}$ under consideration of electromagnetic optimization goals. Under consideration of outliers in the measurement data for the shear strength $\tau_\mathrm{y,I}$, speeds of up
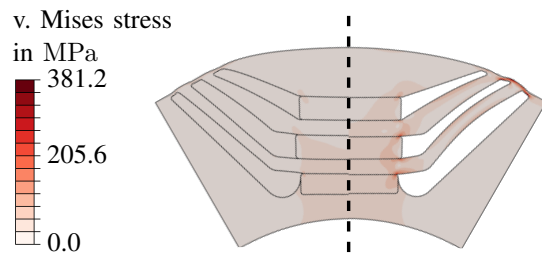
Fig. 9: Comparison of stress in optimized rotor geometries, left: M2, right: M1.

to $v_{\rm rot} = 145\,{\rm m/s}$ or $n = 20\,000\,{\rm 1/min}$ are possible. The measured interface strength shows large variations, depending on sample preparation as well as diverging environmental conditions within the individual test series. One reason for this is the large manual component in processing the specimens. Depending on outside temperature among other parameters, a pre-heated stack of electrical sheet might be inserted into the injection process with differing temperatures, thus yielding distributed results as seen here. An automated process allows for better control of the environmental conditions and may therefore yield more reproducible results.

In addition to the shear strength investigated here, tensile stress tests for the interface between electrical sheet and composite need to be carried out, to define the mechanical limitations imposed upon the system by this stress component and to determine which of these interface loads is the limiting one in terms of speed strength. Once this investigation is concluded, a rotor prototype will be built and the resulting speed strengths of that rotor will be determined experimentally to validate the mechanical path of the design toolchain presented here.

A further improvement of the rotor's speed strength to be validated in the speed tests can be achieved through carbon fiber sheets placed axially between the rotor segments, as is presented in [8]. The combination of the composite injection and these inlays would allow rotor speeds above $n = 20\,000\,{\rm 1/min}$.

REFERENCES

[1] A. Credo, M. Villani, M. Popescu, and N. Riviere, "Application of epoxy resin in synchronous reluctance motors with fluid-shaped barriers for e-mobility," *IEEE Transactions on Industry Applications*, vol. 57, no. 6, pp. 6440–6452, 2021.

[2] Y. Bao, M. Degano, S. Wang, L. Chuan, H. Zhang, Z. Xu, and C. Gerada, "A novel concept of ribless synchronous reluctance motor for enhanced torque capability," *IEEE Transactions on Industrial Electronics*, vol. 67, no. 4, pp. 2553–2563, 2020.

[3] L. Hausmann, M. Waldhof, J. Fischer, W. Wosner, M. Oliveira Flammer, M. Heim, J. Fleischer, and N. Parspour, "Review and enhancements of rotor designs for high speed synchronous reluctance machines," in *2020 10th International Electric Drives Production Conference (EDPC)*. IEEE, 2020, pp. 1–8.

[4] V. Ostovic, "Memory motors," *IEEE Industry Applications Magazine*, vol. 9, no. 1, pp. 52–61, 2003.

[5] K. Sakai, K. Yuki, Y. Hashiba, N. Takahashi, and K. Yasui, "Principle of the variable-magnetic-force memory motor," in *2009 International Conference on Electrical Machines and Systems*. IEEE, 112009, pp. 1–6.

[6] B. Gagas, T. Fukushige, N. Limsuwan, C.-Y. Yu, K. Akatsu, and R. D. Lorenz, "Suggested design space in a pmsm parameter plane for variable flux machines," in *2013 International Electric Machines & Drives Conference*. IEEE, 12.05.2013 - 15.05.2013, pp. 549–556.

[7] M. Ibrahim and P. Pillay, "Design of hybrid variable flux motors for enhanced wide-speed performance," in *2019 IEEE Energy Conversion Congress and Exposition (ECCE)*. IEEE, 29.09.2019 - 03.10.2019, pp. 6046–6053.

[8] J. Kesten, F. Frölich, F. Wittemann, J. Knirsch, F. Bechler, L. Kärger, P. Eberhard, F. Henning, and M. Doppelbauer, "Design approach for a novel multi material variable flux synchronous reluctance machine without rare earth magnets," in *2022 International Conference on Electrical Machines (ICEM)*. IEEE, 952022, pp. 2304–2310.

[9] F. Bechler, J. Kesten, F. Wittemann, F. Henning, M. Doppelbauer, and P. Eberhard, "Simplified modeling of electromagnets for dynamic simulation of transient effects for a synchronous electric motor," *International Journal of Mechanical System Dynamics*, vol. 1, no. 1, pp. 89–95, 2021.

[10] I. A. Melamies, "Adhesion as a benchmark," *IST International Surface Technology*, vol. 10, no. 1, pp. 52–55, 2017.

[11] M. Baytekin-Gerngross, M. Gerngross, J. Carstensen, and R. Adelung, "Making metal surfaces strong, resistant, and multifunctional by nanoscale-sculpturing," *Nanoscale horizons*, vol. 1, no. 6, pp. 467–472, 2016.

[12] M. Müller and D. Herák, "Dimensioning of the bonded lap joint," *Research in Agricultural Engineering*, vol. 56, no. 2, pp. 59–68, 2010.

VI. BIOGRAPHIES

Julius Kesten received his M.Sc in Mechatronics and Information Technology 2020 from the Karlsruhe Institute of Technology (KIT), Germany. Since 2020 he works at the Institute of Electrical Engineering at the KIT. His research interests include the design of synchronous reluctance and variable flux machines and the numerical optimization of electric machines.

David Armbruster received his M.Sc. degree in mechanical engineering in 2020 from University of Stuttgart and is now a Ph.D. student in the Institut für Kunststofftechnik at the University of Stuttgart, starting 2020. His research activities are in the field of injection molding of thermoplastics.

Felix Frölich received his M.Sc. degree in mechanical engineering in 2021 from KIT and is now a Ph.D. student in the Institute of Vehicle System Technology at the KIT, starting 2021. His research focuses are developing simulation models of additive manufacturing processes. In particular, he is working on modeling material extrusion in component size.

Luise Kärger holds a Full Professorship in Digitalization in Lightweight Design and is head of the Lightweight Design Division at the Institute of Vehicle System Technology at KIT. Her research focus is on simulation and optimization of fiber-reinforced composite processes and structures.

Christian Bonten studied mechanical engineering at the Rheinisch-Westfälisch Technische Hochschule Aachen. He was a research assistant at the Essen Chair of Plastics Technology and from 1998 senior engineer in Essen and later at the Institute of Plastics Processing in Aachen. After working in industry with BASF and bioplastics producer FKuR, the mechanical engineer has been professor and head of the Institut für Kunststofftechnik at the University of Stuttgart since 2010. In 2007 he was awarded the Dr. Richard Escales Prize by the Association of German Engineers and Hanser Publishers.

Martin Doppelbauer is full professor since 2011 at the Institute of Electrical Engineering (ETI) at the KIT. He holds a chair for Hybrid Electric Vehicles. Most recently he worked as head of electrical machine development at SEW Eurodrive GmbH in Bruchsal. Martin Doppelbauer is also active in national and international standardization and the chairman of IEC Technical Committee 2 Rotating Electrical Machines.